Available online at www.sciencedirect.com

ScienceDirect

Procedia Structural Integrity 23 (2019) 499–504

Structural Integrity Procedia

www.elsevier.com/locate/procedia

9th International Conference on Materials Structure and Micromechanics of Fracture

Properties of BaTiO3/Al2O3 Laminate Structure by Nanoindentation

Zdeněk Chlup[a]*, Daniel Drdlík[b,c], Martin Fides[d], Alexandra Kovalčíková[d] and Hynek Hadraba[a]

[a]*CEITEC IPM, Institute of Physics of Materials AS CR, v.v.i., Zizkova 22, 616 62 Brno, Czech Republic*
[b]*CEITEC BUT, Brno University of Technology, Purkynova 123, 612 00 Brno, Czech Republic*
[c] *Institute of Materials Science and Engineering, Brno University of Technology, Technicka 2, 616 00 Brno, Czech Republic*
[d] *Institute of Materials Research, Slovak Academy of Sciences, Watsonova 47, 040 01 Košice, Slovak Republic*

Abstract

The proposed material design of $BaTiO_3/Al_2O_3/ZrO_2$ laminate structure predetermined for energy harvesters taking advantage of residual stresses developed during processing was prepared by electrophoretic deposition. The main aim of developed residual stresses is to enhance overall mechanical reliability of piezoceramic functional layers and/or to enhance piezoelectric effects acting in the laminate. The concept of co-sintered $BaTiO_3$ piezo ceramic functional layers with protective ZrO_2 and Al_2O_3 layers is based on strongly bonded layers. In this contribution will be described particular behaviour of the specific material configuration $BaTiO_3/Al_2O_3$ laminate where an interface interlayer among other effects was formed. The influence of sintering conditions on the microstructure development of the laminate as well as the formation of the interlayer was investigated. The relationship between observed microstructural changes and resulting mechanical properties as hardness and indentation elastic modulus was analyzed by means of nanoindentation technique. The cracks propagation through the individual layers and specific formed interfaces were observed and analyzed. The crack deflection due to the presence of developed residual stresses during the cooling stage of sintering as well as the consequence of microstructural changes on mechanical properties was confirmed.

Keywords: Piezoceramic; barium titanate; laminate; nanoindentaion; mechanical properties.

*Corresponding author. Tel.: 420-532-290-335.
E-mail address: chlup@ipm.cz

10.1016/j.prostr.2020.01.135

1. Introduction

With the development of smart electronic devices, the need for localised low and ultra-low power sources becoming urgent. Piezoelectric energy harvesters transforming ubiquitous vibrations to the electric energy can be one of the candidates (Bai et al., 2018; Hadas, Janak, & Smilek, 2018; Li, Gao, & Cong, 2018). The proposed material design of $BaTiO_3/Al_2O_3/ZrO_2$ laminate structure predetermined for energy harvesters. The lead-free BaTiO3 piezoceramic seems to be a potentially material replacing nowadays used PZT with some drawbacks in the processing and efficiency. The concept of co-sintered $BaTiO_3$ piezo ceramic functional layers with protective ZrO_2 and Al_2O_3 layers is based on strongly bonded layers (Gao, Xue, Liu, Zhou, & Ren, 2017; Zych, Wajler, & Kwapiszewska, 2016).

Nomenclature

E_{IT}	Indentation Elastic Modulus
H	Nanoindentation Hardness
ρ_{rel}	Relative Density
T_{sint}	Sintering Temperature

The advantage of the presence of residual stresses developed during processing is to enhance overall mechanical reliability of piezoceramic functional layers and/or enhance piezoelectric effects acting in the laminate (Bermejo et al., 2006; Lugovy et al., 2005; Sglavo, Paternoster, & Bertoldi, 2005).

The particular behaviour of the material configuration of $BaTiO_3/Al_2O_3$ laminate with a specific interface interlayer will be described in this contribution.

2. Experimental

Commercial alumina (~470 nm, Malakoff, USA) and barium titanate (~500 nm, ABCR, Germany) powders were used for the electrophoretic deposition (EPD) of the layered structure. The laminate structure was fabricated by moving of a deposition electrode from one suspension to another one(H. Hadraba, Maca, & Cihlar, 2004). The suspensions contained 15 wt.% of powder, 12.75 wt% of stabilizer - monochloroacetic acid (Merck, Germany) and 72.25 wt.% of 2-propanol. The nominal thicknesses of $BaTiO_3$ and Al_2O_3 layers were 100 μm and 200 μm, respectively. The deposition times of layers varied and they depended on the kinetic study of individual materials (Hynek Hadraba et al., 2013). The laminate was dried for 24 h with consequent annealing at 800°C for 1 h in the air to burn out the organic additives. The ceramic laminate was sintered at 1300°C, and 1350°C for 1h in the air. The laminate sintered at 1350°C was suitable for nanoindentation experiments using a Berkovich tip on an Agilent G200 in CSM (continuous stiffness measurement) mode into the maximum depth of 1200nm. The depth range of 800-1200 nm was used for calculation of average hardness and modulus. The microstructure and indentation imprints were observed using the scanning electron microscope Lyra 3 XMU (Tescan, Czech Republic) and the chemical analysis was conducted using EDS X-Max80 (Oxford Instruments, UK).

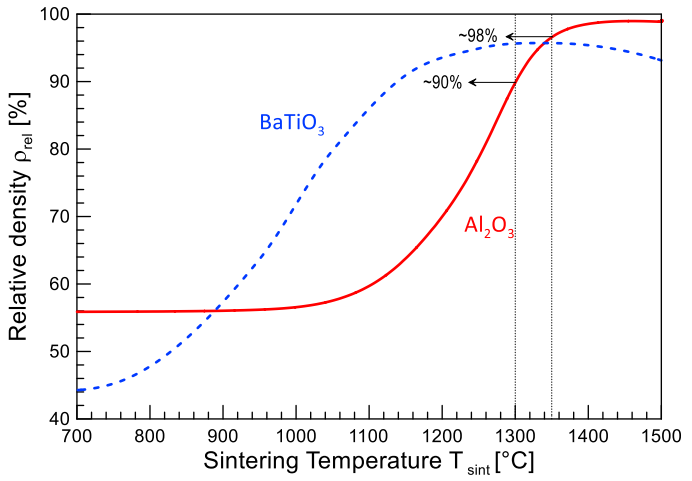

Fig. 1. Schematic sintering curves for Al_2O_3 and $BaTiO_3$ ceramics with marked sintering temperatures.

3. Results and Discussion

Two symmetrical laminates consisting of seven layers (three $BaTiO_3$ and four Al_2O_3 layers) were successfully prepared via alternating EPD. The variation in the sintering temperature led to the significant microstructural changes where differences between sintering behaviour of Al_2O_3 and $BaTiO_3$ take place. The example of sintering curves for both materials can be found in Fig. 1 where $BaTiO_3$ sinter at lower temperatures then Al_2O_3 reaches lower final densities of green bodies. Additionally, there exist effects originating from differences in initial densities caused by the effectiveness in the deposition mechanism of powder particles for each material. Obviously, the only porous Al_2O_3 layer can be obtained in case of the sintering temperature T_{sint}=1300°C in comparison with the sintering at 1350°C where nearly fully dense Al_2O_3 material can be expected according to the sintering curves (see Fig. 1). It is necessary to mention that for the demonstration reasons are not taken in to account so-called co-sintering effects(Chlup et al., 2014; Maca, Pouchly, Drdlik, Hadraba, & Chlup, 2017). They can slightly change the mentioned situation with the probable formation of some porosity in the $BaTiO_3$ layer due to constrained sintering (free shrinkage is not possible) and slightly higher density of the Al_2O_3 layer (stress assisted sintering) can be expected.

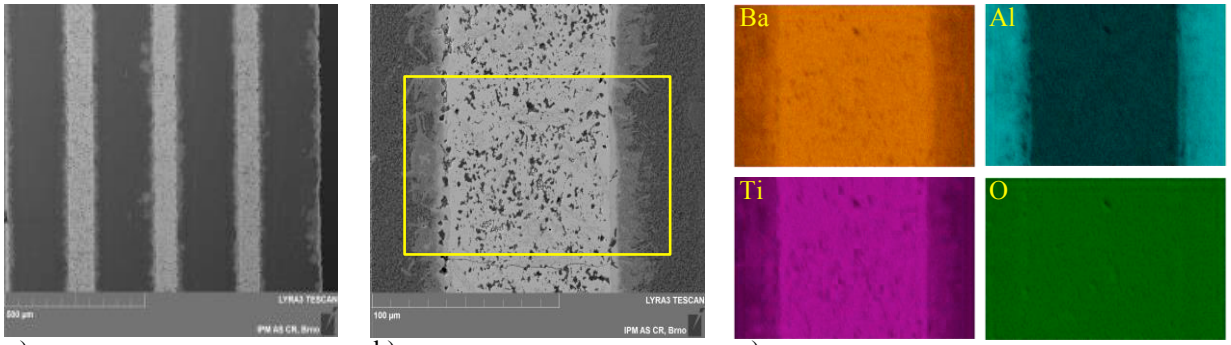

Fig. 2. The microstructures of prepared laminate sintered at 1300°C a) an overview BSE (electrode placement left, free surface right), b) detail of one BaTiO3 layer with a marked rectangle of EDS mapping, and c) distribution of main elements from EDS mapping.

The example of obtained microstructure for laminate sintered at 1300°C is shown in Fig. 2. The layered structure is slightly uneven as can be seen in Fig. 2a) where $BaTiO_3$ layers have lower thickness with the increasing distance from the electrode. This effect is caused by the discrepancy of designed and real deposition kinetics and it can be further enhanced as was reported elsewhere (Hynek Hadraba et al., 2013). The relatively low density obtained for sintering at 1300°C not allow a further investigation by the nanoindentation technique. On the other hand, there was no strong effect of the material interaction near the layers interface as is noticeable mainly from the backscatter electron image shown in Fig. 2b) and corresponding EDS maps shown in Fig. 2c) where penetration of Ba and Ti to the Al_2O_3 layer is obvious. It is a sign of chemical interaction of $BaTiO_3$ in the Al_2O_3 layers where the oxygen content seems to be unchanged. The situation was significantly changed when the sintering temperature increased to 1350°C. An example of the microstructure in the vicinity of Al_2O_3/$BaTiO_3$/Al_2O_3 layers interfaces is illustrated in Fig. 3a) where nearly complete Al_2O_3 layer is infiltrated by Ba and Ti similarly to the previously described case. The differences can be recognised in the formation of some new phase in the form of the interlayer surrounding the $BaTiO_3$ layer. The grain size of BaTiO3 is increased significantly to the size of approximately 10µm.

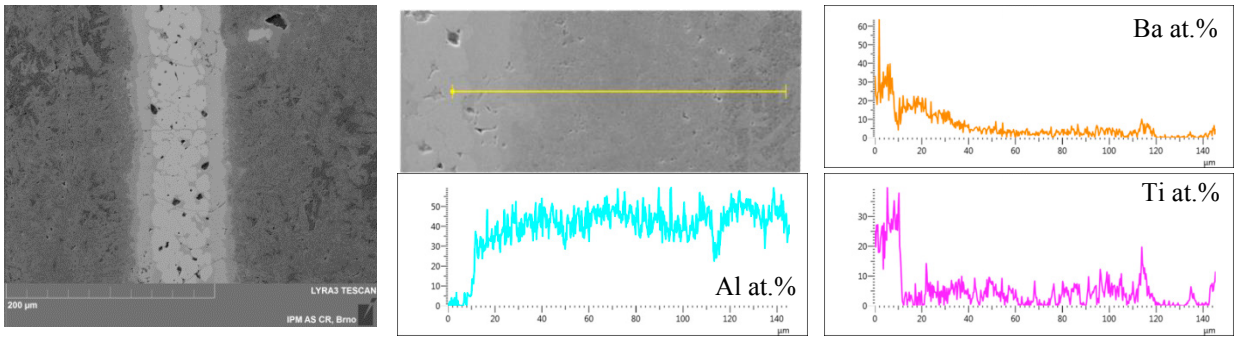

Fig. 3. The microstructures of prepared laminate at 1350°C a) a view on BaTiO layer, b) detail of interface area between $BaTiO_3$ (left) and Al_2O_3 (right) layers with a marked EDS line scan and resulting profiles for relevant elements.

The chemical microanalysis presented in Fig. 3b) proved the presence of barium and titanium through the whole Al_2O_3 layer. The formed interface had a significantly higher content of barium and titanium than would be expected for $BaTiO_3$. The interlayer phase can be $BaAl_2O_4$ and $BaAl_6TiO_{12}$ or $Ba_4Ti_{10}Al_2O_{27}$ according to the literature data (Chen & Yang, 1997; Rattanachan, Miyashita, & Mutoh, 2004). The nanoindentation was used to monitor mechanical response with the distance from the $BaTiO_3$ layer. The results are shown in Fig. 4 where dashed vertical lines represent the theoretical layer interface and the dash-and-dot lines represent the symmetry axes of the layers. The hardness that increased continuously from the $BaTiO_3$ layer to be maximum of hardness that was not located in the centre of the Al_2O_3 layer as one can have expected but nearby. In the centre of the Al_2O_3 layer was identified the local minimum caused by the presence of porosity. This finding is in good agreement with the penetration of Ba and Ti nearly to the central part of the Al_2O_3 layer increasing the density by filling of preexisting pores. The position dependence of indentation elastic modulus is shown in Fig. 4b). The same trend as for hardness can be observed with the exception of values obtained in the vicinity of the formed new interface layer. In general, the hardness values are rather similar to the Al_2O_3 contrary to the indentation elastic modulus which is close to the $BaTiO_3$ layer.

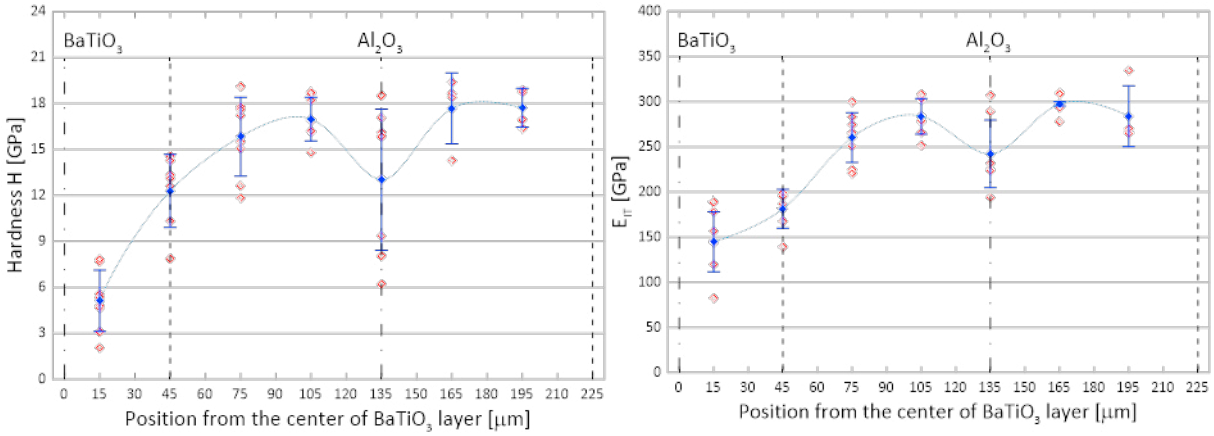

Fig. 4. Dependence of a) hardness, and b) indentation elastic modulus on the position from the centre of $BaTiO_3$ layer.

The detailed analysis of chemical composition in the places of individual indents was conducted with the aim to identify dependence of the selected elements on hardness. The dependence of individual elements on the position from the centre of $BaTiO_3$ layer is shown in Fig. 5a). Obviously, the same content of Ba and Ti found in $BaTiO_3$ layer was changed in favour of Ba in the formed interface layer and further in favour of Ti within the Al_2O_3 layer. The content of individual elements was however locally changed when a closer look is taken. The detailed EDS mapping within one indentation imprint placed in the Al_2O_3 layer was conducted with results shown in Fig. 5b). The EDS maps show

the local crystallinity of the microstructure containing various chemical composition. This means that not only one phase was formed but many transitional phases in the form of sub-micron crystals were created depending on the distance from the $BaTiO_3$ source.

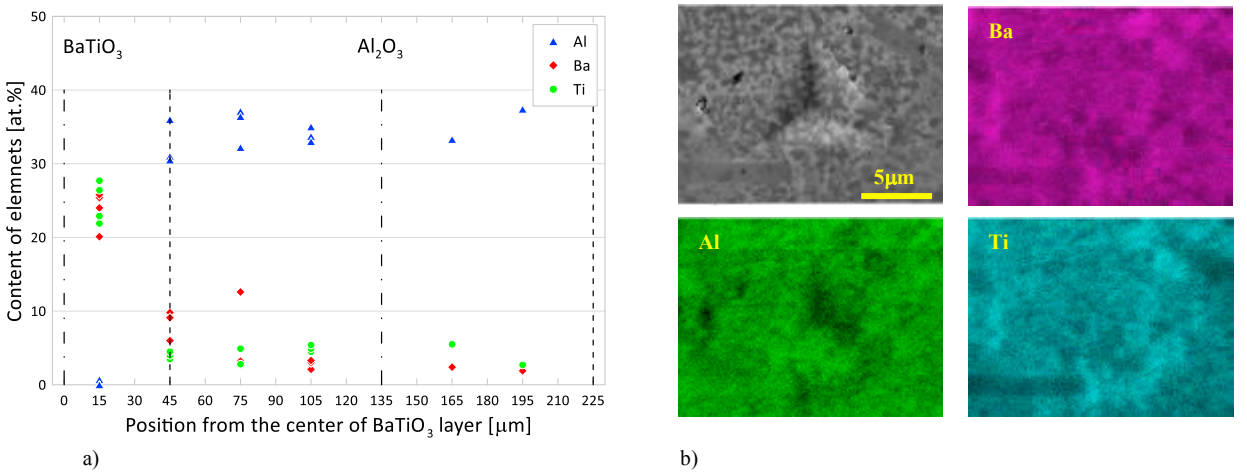

Fig. 5. Dependence of a) individual elements on the position from the centre of $BaTiO_3$ layer, and b) close look on the chemical composition within one indent in the distance of 105µm.

The fracture behaviour by the observation of indentation cracks was identified. The cracks formed within $BaTiO_3$ layer propagated perpendicularly to the layer interfaces were deflected when reaching such layer interface. The cracks propagation through the specifically formed interface interlayer was strongly inclined to the interface direction and then propagated to the Al_2O_3 layer where they were stopped (see Fig. 6). This behaviour can be ascribed to the presence of developed compressive residual stresses in the Al_2O_3 layer as well as an increase of elastic properties as was predicted and previously demonstrated on various systems (Bermejo, Pascual, Lube, & Danzer, 2008; Hbaieb, McMeeking, & Lange, 2007; Ševeček, Bermejo, & Kotoul, 2013).

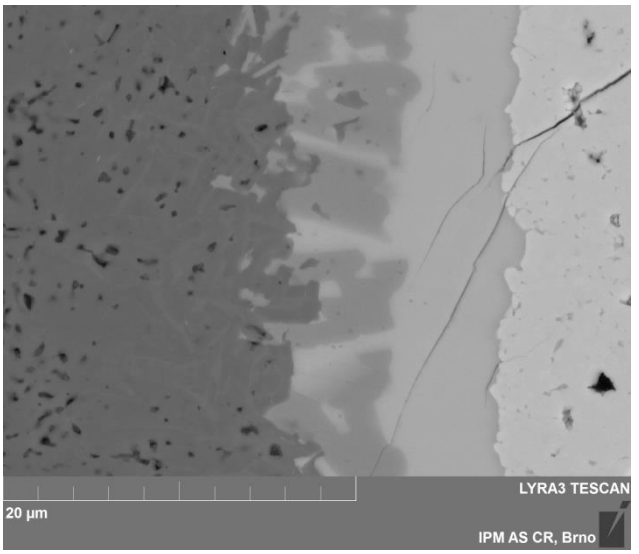

Fig. 6. SEM micrograph in backscattered electrons mode showing an example of crack propagation from the BaTiO3 layer to the interlayer where strong deflection can be observed.

4. Conclusions

The influence of sintering conditions on the development of microstructure laminate as well as the formation of interlayer was investigated. The relationship between observed microstructural changes and resulting mechanical properties showed a discrepancy in the formed interlayer where hardness was close to the Al_2O_3 layer contrary to the

indentation elastic modulus inclined to the values of $BaTiO_3$. Microstructural changes in the laminated piezoceramic $BaTiO_3/Al_2O_3$ structure occurred during the sintering process were described and the mechanical response was determined by means of nanoindentation. The formation of many transitional phases in the form of sub-micron crystals depending on the distance from the $BaTiO_3$ source was found. The cracks propagation through the individual layers and specific formed interfaces were observed and analyzed. The crack deflection due to the presence of developed residual stresses during the cooling stage of sintering as well as the consequence of microstructural changes on mechanical properties was confirmed.

Acknowledgements

This research was supported by the Czech Science Foundation under the project GAP 17-08153S and the infrastructure supported by project CEITEC 2020 (LQ1601).

References

Bai, Y., Tofel, P., Hadas, Z., Smilek, J., Losak, P., Skarvada, P., & Macku, R. (2018). Investigation of a cantilever structured piezoelectric energy harvester used for wearable devices with random vibration input. *Mechanical Systems and Signal Processing, 106*, 303-318. doi:https://doi.org/10.1016/j.ymssp.2018.01.006

Bermejo, R., Pascual, J., Lube, T., & Danzer, R. (2008). Optimal strength and toughness of Al(2)O(3)-ZrO(2) laminates designed with external or internal compressive layers. *Journal of the European Ceramic Society, 28*(8), 1575-1583. doi:10.1016/j.jeurceramsoc.2007.11.003|10.1016/j.jeurceramsoc.2007.11.003

Bermejo, R., Torres, Y., Sanchez-Herencia, A., Baudin, C., Anglada, M., & Llanes, L. (2006). Residual stresses, strength and toughness of laminates with different layer thickness ratios. *Acta Materialia, 54*(18), 4745-4757. doi:10.1016/j.actamat.2006.06.008|10.1016/j.actamat.2006.06.008

Chen, X. M., & Yang, B. (1997). A new approach for toughening of ceramics. *Materials letters, 33*(3-4), 237-240.

Chlup, Z., Hadraba, H., Drdlik, D., Maca, K., Dlouhy, I., & Bermejo, R. (2014). On the determination of the stress-free temperature for alumina-zirconia multilayer structures. *Ceramics International, 40*(4), 5787-5793. doi:10.1016/j.ceramint.2013.11.018

Gao, J., Xue, D., Liu, W., Zhou, C., & Ren, X. (2017). Recent Progress on BaTiO3-Based Piezoelectric Ceramics for Actuator Applications. *Actuators, 6*(3). doi:10.3390/act6030024

Hadas, Z., Janak, L., & Smilek, J. (2018). Virtual prototypes of energy harvesting systems for industrial applications. *Mechanical Systems and Signal Processing, 110*, 152-164. doi:https://doi.org/10.1016/j.ymssp.2018.03.036

Hadraba, H., Drdlik, D., Chlup, Z., Maca, K., Dlouhy, I., & Cihlar, J. (2013). Layered ceramic composites via control of electrophoretic deposition kinetics. *Journal of the European Ceramic Society, 33*(12), 2305-2312. doi:10.1016/j.jeurceramsoc.2013.01.026

Hadraba, H., Maca, K., & Cihlar, J. (2004). Electrophoretic deposition of alumina and zirconia - II. Two-component systems. *Ceramics International, 30*(6), 853-863. doi:10.1016/j.ceramint.2003.09.020

Hbaieb, K., McMeeking, R. M., & Lange, F. F. (2007). Crack bifurcation in laminar ceramics having large compressive stress. *International Journal of Solids and Structures, 44*(10), 3328-3343. doi:10.1016/j.ijsolstr.2006.09.023

Li, P., Gao, S., & Cong, B. (2018). Theoretical modeling, simulation and experimental study of hybrid piezoelectric and electromagnetic energy harvester. *AIP Advances, 8*(3), 035017. doi:10.1063/1.5018836

Lugovy, M., Slyunyayev, V., Orlovskaya, N., Blugan, G., Kuebler, J., & Lewis, M. (2005). Apparent fracture toughness of Si3N4-based laminates with residual compressive or tensile stresses in surface layers. *Acta Materialia, 53*(2), 289-296. doi:10.1016/j.actamat.2004.09.022

Maca, K., Pouchly, V., Drdlik, D., Hadraba, H., & Chlup, Z. (2017). Dilatometric study of anisotropic sintering of alumina/zirconia laminates with controlled fracture behaviour. *Journal of the European Ceramic Society, 37*(14), 4287-4295. doi:10.1016/j.jeurceramsoc.2017.04.030

Rattanachan, S., Miyashita, Y., & Mutoh, Y. (2004). Effect of polarization on fracture toughness of BaTiO3/Al2O3 composites. *Journal of the European Ceramic Society, 24*(5), 775-783. doi:https://doi.org/10.1016/S0955-2219(03)00319-4

Sglavo, V. M., Paternoster, M., & Bertoldi, M. (2005). Tailored Residual Stresses in High Reliability Alumina-Mullite Ceramic Laminates. *Journal of the American Ceramic Society, 88*(10), 2826-2832. doi:10.1111/j.1551-2916.2005.00479.x

Zych, Ł., Wajler, A., & Kwapiszewska, A. (2016). Sintering Behaviour of Fine Barium Titanate (BaTiO 3) Powders Consolidated with the Pressure Filtration Method. *JOURNAL OF CERAMIC SCIENCE AND TECHNOLOGY, 7*(3), 277-287.

Ševeček, O., Bermejo, R., & Kotoul, M. (2013). Prediction of the crack bifurcation in layered ceramics with high residual stresses. *Engineering Fracture Mechanics, 108*, 120-138. doi:https://doi.org/10.1016/j.engfracmech.2013.03.013